eJNDT e-Journal of Nondestructive Testing - ISSN 1435-4934 - www.ndt.net

EWGAE 2024
36th Conference of the European Working Group on Acoustic Emission

Mechanical Robustness Analysis of Semiconductors with a Single Needle Probe Card Using Acoustic Emissions

Florian TREMMEL [1], Oliver NAGLER [1], Christoph KUTTER [2], Rainer HOLMER [3]
[1] Infineon Technologies AG, Department Test Technology and Innovation, 85579 Neubiberg, Germany, Florian.Tremmel@infineon.com, Oliver.Nagler@infineon.com
[2] Fraunhofer Institute for Electronic Microsystems and Solid State Technologies EMFT, 80686 Munich, Germany and University of the Bundeswehr Munich, Institute of Physics, 85579 Neubiberg, Germany, Christoph.Kutter@emft.fraunhofer.de
[3] Ostbayerische Technische Hochschule Regensburg, Faculty of Electrical Engineering and Information Technology, 93053 Regensburg, Germany, Rainer.Holmer@oth-regensburg.de

Abstract. Wafer testing is a process step in the semiconductor manufacturing chain at which inside a wafer prober small probe tips are pressed onto contact pads on a chip surface to perform an electrical functionality check. An acoustic emission (AE)-based crack detection method is used to define the mechanical load limits of the chips during this step. However, the current, customized test setup leads to different measurement conditions compared to the productive test environment. This can cause a falsification of the obtained measurement results. This study presents a solution by performing the AE test method inside a wafer prober which leads to more realistic measurement conditions and increases the availability of the test method. To enable the integration into a wafer prober, a dual cantilever probe with an integrated AE and force sensor has been developed. Also, a customized solution for the data processing and recording is shown. To prove the functionality of the whole test bench, crack probability tests are performed and compared to results with the old setup. Despite having a lower signal-to-noise ratio (SNR), the new setup generates nearly identical clusters of the AE signals and similar crack probability distributions. This confirms the functionality of the developed measurement setup and the applicability of an AE-based crack detection method inside a wafer prober.

Keywords: Wafer testing, fracture load limit, acoustic emission, crack probability distribution.

1. Introduction

Indentation testing is usually coupled with acoustic emission (AE) analyses to provide a defined mechanical load with the indenter and use the generated AE signals to define or gain further insight into the material properties of the contacted test specimen [1] [2] [3]. During

https://doi.org/10.58286/30254

chip production, this combination of test methods can also be used to define fracture load limits for the wafer testing process step [4]. In this semiconductor manufacturing step inside a wafer prober small, elastic probe tips are pressed onto contact pads on the wafer surface. This allows to check the electrical functionality of the tested device in an early manufacturing phase. To make sure that the multi-layer structure under the pad is not damaged, load limits have to be defined in advance.

This is done by intentionally overloading the contact pads and searching for appearing cracks. Implementing a non-destructive AE-based crack detection method to replace invasive optical methods has led to a reduced processing time and a higher accuracy. The main measurement component to execute the tests is shown in Fig. 1. It uses a rigid steel indenter with a small diamond tip to imitate the probe tips and catches the generated acoustic crack signals with an AE sensor attached to its end. The patented sensor indenter (SI) system [5] is mounted on a load cell to assign the applied contact force to the recorded AE signals.

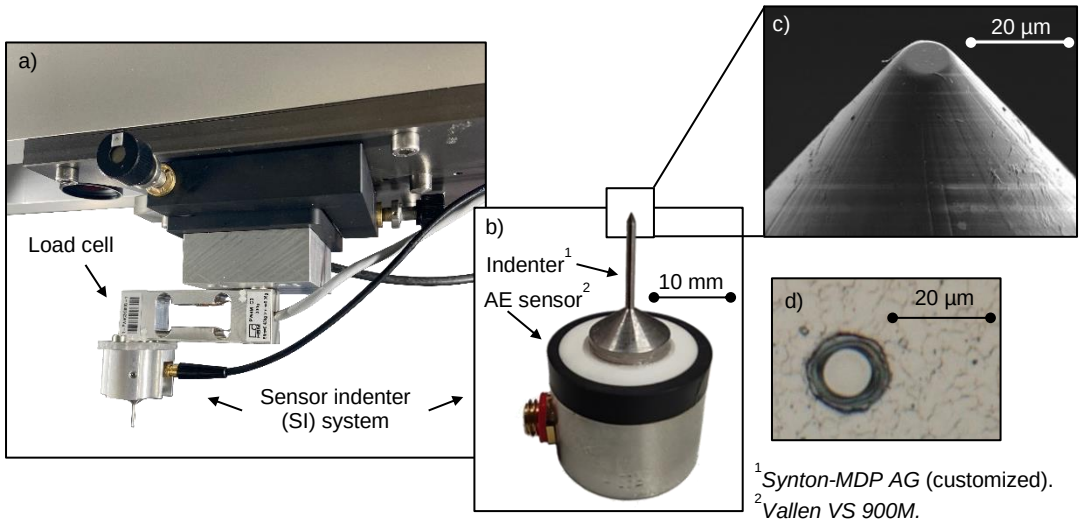

Fig. 1. Measurement setup for AE-based crack probability analyses of multilayer semiconductor substrates. a) Sensor indenter (SI) system together with the load cell used for contact force detection. b) The SI system and its components are shown in detail. c) High resolution SEM image of the diamond tip of the indenter. d) Remaining imprint of the SI system on a test substrate.

The functionality and accuracy of the AE-based crack detection has already been proven over time in several high statistic measurement series and optical cross correlations [6]. However, the test bench has some limitations regarding the replication of the test parameters that occur during productive wafer testing in a wafer prober. The limitations are caused by specific prober features like temperature control, high probing speed, etc. but also by differing mechanical interactions between the probe/indenter tip and the wafer surface. Productive wafer testing probes are more elastic and generate a different imprint shape compared to the steel indenter (Fig. 2). These deviations could lead to a different crack formation and a falsification of the obtained contact force limits.

This study presents a way to overcome these limitations by implementing the AE-based crack detection method inside a commercial wafer prober. To enable this, the design of the SI system was changed and brought closer to a productive cantilever probe with smaller dimensions, a reduced stiffness and a more realistic probe mark including scrubbing. The new cantilever design also includes a customized force and AE sensor. To improve the quality of the sensor signals, for the data preparation and recording own solutions have been developed. To confirm the functionality of all developed components, at the end of this paper crack probability analyses are performed inside a wafer prober and compared to previously obtained results with the old setup in Fig. 1.

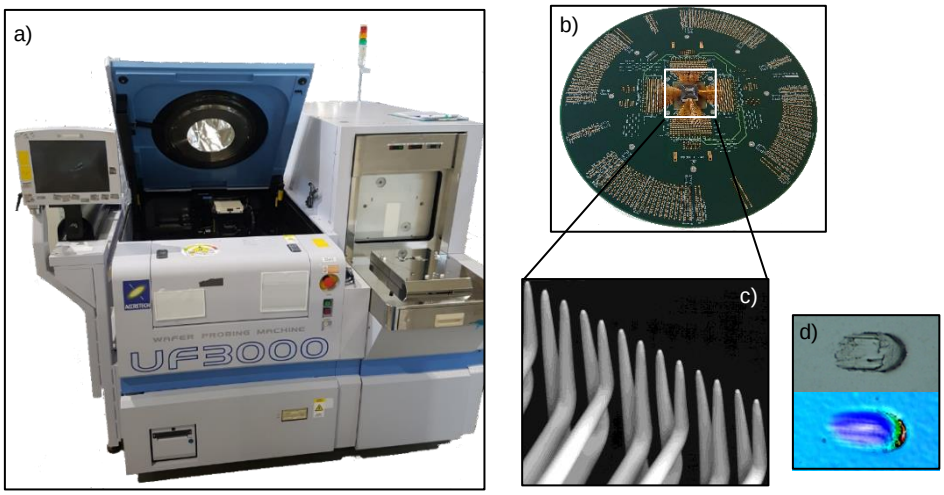

Fig. 2. a) Wafer prober used for productive wafer testing. b) Probe card that contains probes for generating an electrical contact with the tested chip device. c) High resolution REM image of the cantilever probe tips. d) Remaining imprint of a cantilever probe on a test substrate (+ coloured topographic image).

2. Measurement setup

2.1 New Sensor Element and Wafer Prober Integration

The core component of the new measurement setup is the developed sensor cantilever combination (SCC) shown in Fig. 3a). The dual cantilever design enables an easy adjustment of the bending stiffness and scrubbing behaviour. At the beginning of the cantilever arm, at the area of maximum strain, four strain gauge elements (*Althen GmbH*, *FLAB-1-350-17*) are glued. They are arranged as a full Wheatstone bridge and form the force sensor. At the end of the cantilever arm, an indenter with a diamond tip can be mounted via a threaded joint. On top of the detachable indenter, a piezoelectric disc with wrap-around electrodes (*PI Ceramic GmbH*, customized) is glued establishing a good mechanical contact but no electrical connection to the indenter. The SCC is placed on a small PCB on which both sensor signals are transferred to an ethernet port for easier signal transmission (Fig. 3b)). [7]

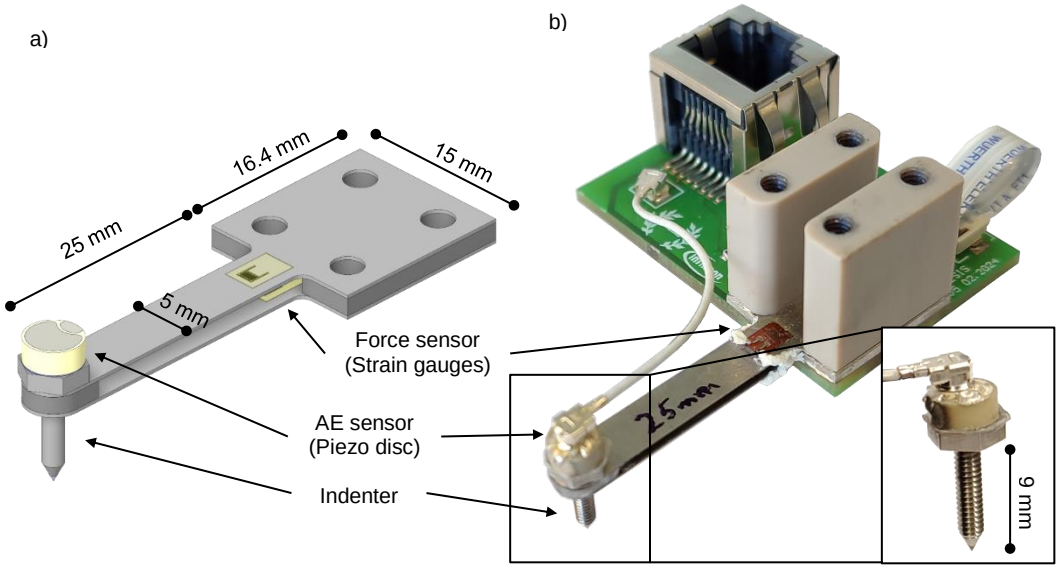

Fig. 3. Developed sensor cantilever combination (SCC). a) 3D simulation model with integrated AE and force sensor elements. b) SCC prototype mounted on a PCB to transfer the sensor signals to an ethernet port.

In Fig. 4 the customized mechanical integration of the SCC into the wafer prober is displayed step by step. The combination of SCC and mounting PCB is connected via a mini-manipulator to a round plastic plate (probe card). The manipulator is used to correct any tilting of the indenter and achieve a perpendicular alignment to the test substrate. An aluminium framework (stiffener) is attached to the probe card to increase its stiffness. The probe card is placed on a probe card holder with alignment pins, that keep the probe card in position. Lever clamps fix the probe card in vertical direction.

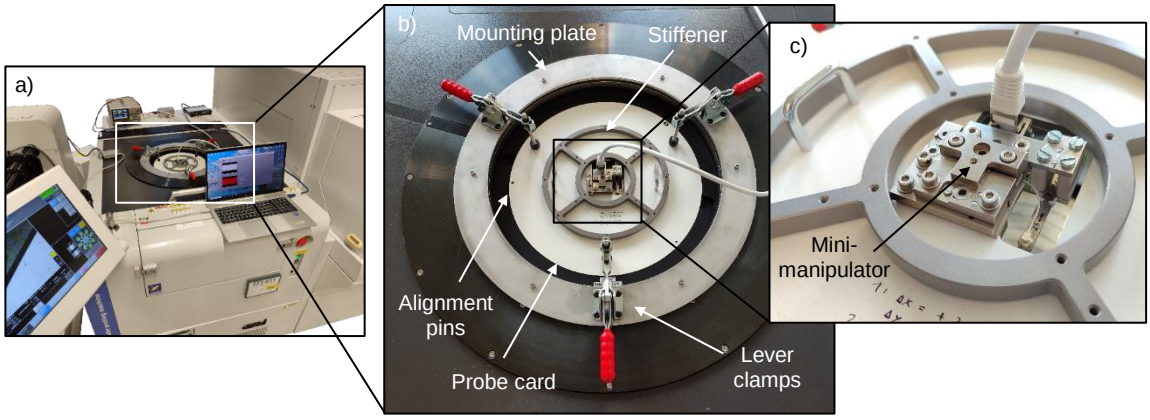

Fig. 4. a) Wafer prober with integrated AE probe card. b) Close up view of the single needle probe card and its installation into the wafer prober. c) Connection between probe card and SCC via mini-manipulator.

The interaction and data flow of the different components of the measurement setup is shown in Fig. 5. The output signals of AE and force sensor are transferred via ethernet cable to an analogue amplifier and filter module. The improved sensor signals are forwarded to a PC-based oscilloscope (*Pico Technology, PicoScope 5443D*). The settings and recording of the oscilloscope as well as the movements of the wafer prober are controlled with a developed *LabVIEW* program. A separate *MATLAB* program is used to filter the collected AE sensor data for relevant crack signals and fit a probability distribution to them.

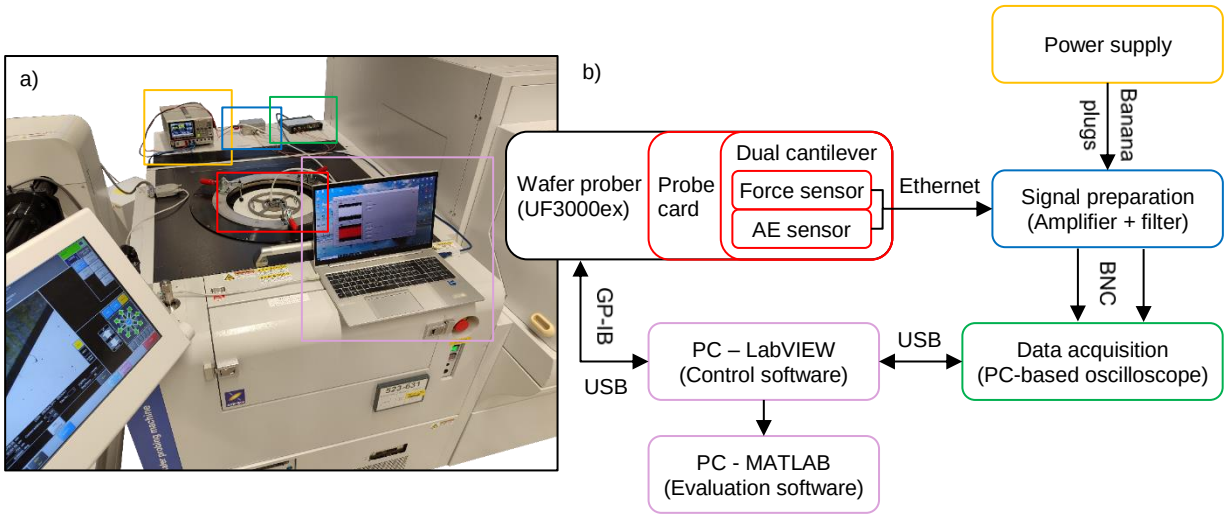

Fig. 5. Schematic overview of the internal structure of the new test bench. a) Picture of the measurement system with marked components. b) Data flow diagram of the different components.

2.2 Signal Preparation

The module for the signal preparation contains analogue filter and amplifier electronics for the AE and force sensor signals. Both channels have two operational amplifier stages and a dual in-line package (DIP) switch integrated into the second stage to adjust their total gains. The AE chain uses a single-ended charge amplifier in the first stage and a non-inverting

amplifier in the second stage. Both amplifier stages cover the frequency range between 40 kHz and 5.5 Mhz. Afterwards, a modular 6th-order LC bandpass filter narrows down the -3 dB passband between 50 kHz and 2 MHz with its steep filter slopes. The force chain uses an instrumentation amplifier in the first stage and also a non-inverting amplifier in the second stage. It doesn't have an additional filter but the two amplifier stages create a lowpass characteristic with a cutoff frequency at around 2 kHz. [7]

2.3 Data Acquisition

The previous setup in Fig. 1 utilizes an *AMSY-6* AE measurement system with an *ASIP-2* acoustic signal processor from *Vallen Systeme GmbH* for the data acquisition. To have comparable end results, the acquisition settings are replicated as close as possible with the PC-based oscilloscope in the new setup. The sample rate of the oscilloscope input channels (AE and force signal) is set to 2 MHz with a 14-bit resolution. Looking at an exemplary AE signal in Fig. 6, a windows-based trigger approach of the AE signals is used. The total signal length is variable depending on t_{dur} with a fixed value of t_{pre} (20 µs) and t_{post} (200 µs). The force sensor channel is permanently recorded with a 2 MHz sample rate but the data points are averaged down to a 2 kHz rate to keep the corresponding output files at a reasonable size. The force curves (Fig. 7) show small disturbances during the contact cycles caused by vibrations of the wafer prober. They can be ignored as the disturbances are too small to have a relevant influence on the contact force determination. They also don't trigger an AE signal generation as their frequency spectrum is below the passband of the AE amplifier chain. With help of the recorded force curves and a predefined threshold value, the *LabVIEW* program recognizes individual contact cycles, separates the force curves accordingly and assigns the detected AE signals to them.

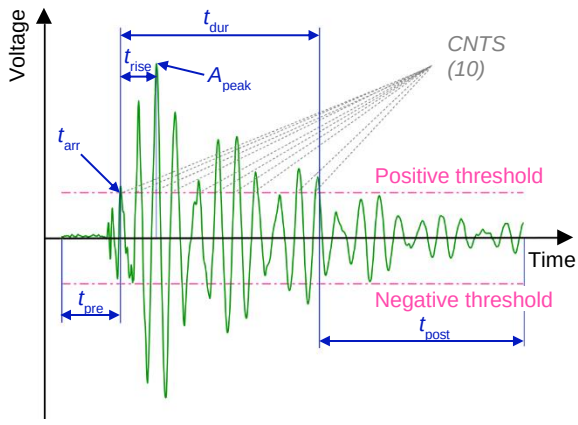

Fig. 6. Different parameters of an exemplary AE signal. Two threshold levels are used to form a windows-based trigger approach.

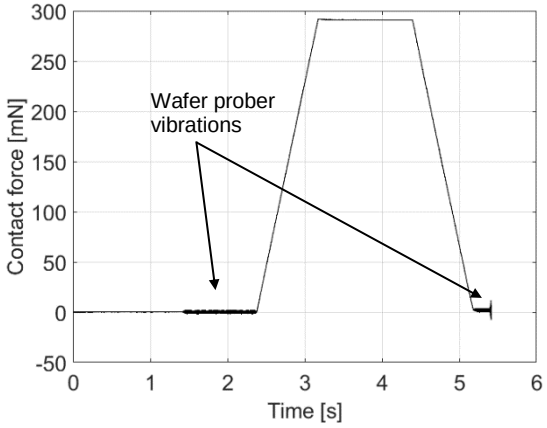

Fig. 7. Recorded contact force curve. The highlighted disturbances are caused by wafer prober vibrations due to the vertical movement of the substrate holder.

2.4 Data Evaluation

Every contact cycle generates one text file containing the contact force curve and several additional text files containing one AE event each. As solely the first crack signal is relevant for the later fit of the crack probability distribution, a sufficient number of contact cycles has to be conducted to obtain a statistically reliable database. To separate crack signals from AE hits caused by plastic deformation, mechanical disturbance etc., different parameters are extracted as a representative for each AE hit. In this study the applied contact force and the AE signal energy are used to filter out the crack signals. Other signal parameters like the frequency spectrum or the rise time t_{rise} are mainly defined by the design of the indenter and

piezo element and contain therefore no valuable information about the signal source. The signal energy E_{AE} is calculated with the AE sensor voltage $u(t)$ according to

$$E_{AE} = \int_{t_{arr}}^{t_{arr}+t_{dur}+t_{post}} \frac{u(t)^2}{10\ k\Omega}\, dt. \tag{1}$$

A theoretical resistance value of 10 kΩ is selected for this calculation. As $u(t)$ describes the sensor output signal, the recorded AE hits are divided by the preamplifier gain. Also, in this study signal energy is described in the quantity "energy units" (eu) [8] whereby

$$1\ eu = 1 \cdot 10^{-18}\ J. \tag{2}$$

In the first step, only the AE signals obtained during the loading phase of the contact cycles are filtered out and further analysed. After that, manually lower limits for the contact force and signal energy are selected after optical inspection of the cluster distribution of the AE signals, as shown in Fig. 8a). Previous investigations have shown that the high energetic AE hits at low contact forces aren't generated by a crack formation but by plastic deformations inside the top metal layer of the substrate. Inside the selected area, the first appearing signal of every contact cycle is detected and plotted against the applied contact force F to get the crack probability density distribution in Fig. 8b). In the next step, a three-parametric Weibull distribution P_{WB} [9] is fitted over the cumulative data, following the equation

$$P_{WB}(F) = 1 - e^{-\left(\frac{F-F_u}{F_o}\right)^m}. \tag{3}$$

The Weibull modulus m defines the spreading of the crack probability. The parameter F_u, which is added compared to the two-parametric Weibull distribution, implements a lower force limit for the appearance of cracks. The parameter F_o affects the position of the distribution function whereby the force value $F_o + F_u$ always shows a crack probability of 63%. A fit of the crack probability function P_{WB} can be seen in Fig. 8c). Earlier investigations have shown that the three-parametric Weibull distribution is best suited for describing the statistical crack behaviour of mixed metal-insulator multilayer substrates, especially at low contact forces [10]. This is important as the fitted function is extrapolated to low probability values of around 1 ppm. This is necessary to define a critical contact force limit that fulfils the high-quality standards of semiconductor products during wafer testing.

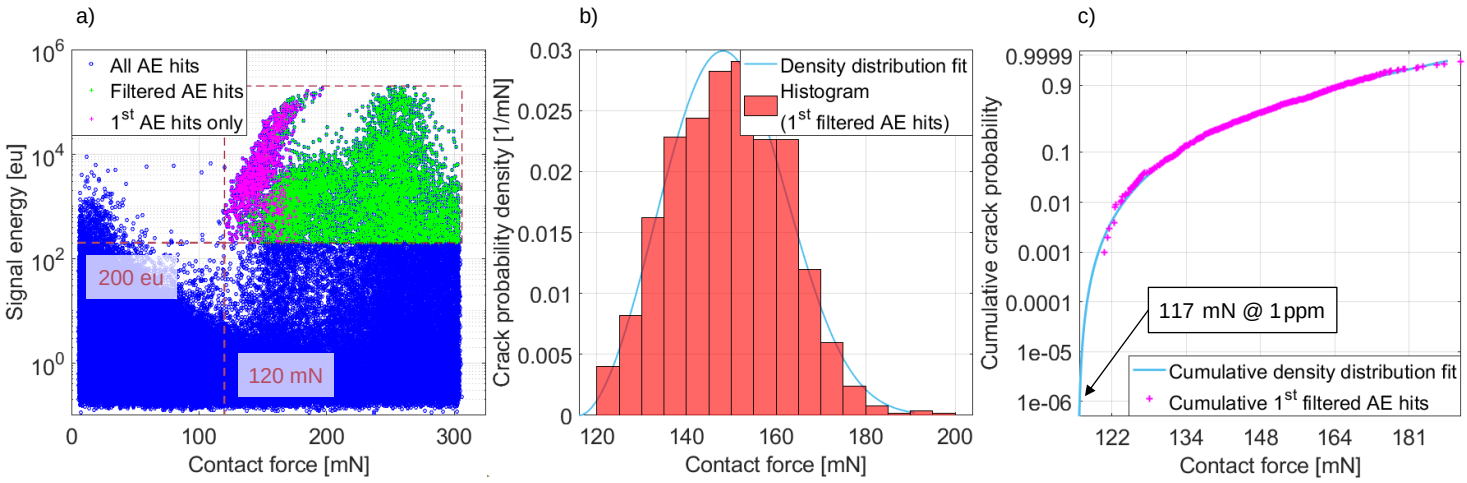

Fig. 8. Process steps for the evaluation of the AE data of a high statistical crack probability analysis (in this example accumulated AE hits of 1000 contact cycles). a) Filtering of the first appearing AE crack signals with lower limits for the signal energy and contact force (200 eu and 120 mN). b) Visualization of the measured crack probability density as a histogram including a fit with a three-parametric Weibull distribution. c) Plot of the cumulative 1st filtered AE hits with a fitted three-parametric Weibull distribution. Extrapolation of the distribution to a 1 ppm crack probability. Detected contact force limit at 117 mN.

3. Measurement Settings and Results

To check the applicability of the new measurement system, a crack probability analysis is repeated with both the old (Fig. 1) and new test setup (Fig. 5). The results of the first one after 1000 load cycles have already been shown in Fig. 8. A force limit of 117 mN with a crack probability of 1 ppm has been extrapolated. The corresponding test substrate and contact pads including probe marks as well as a schematic overview of the stack layout underneath are shown in Fig. 9.

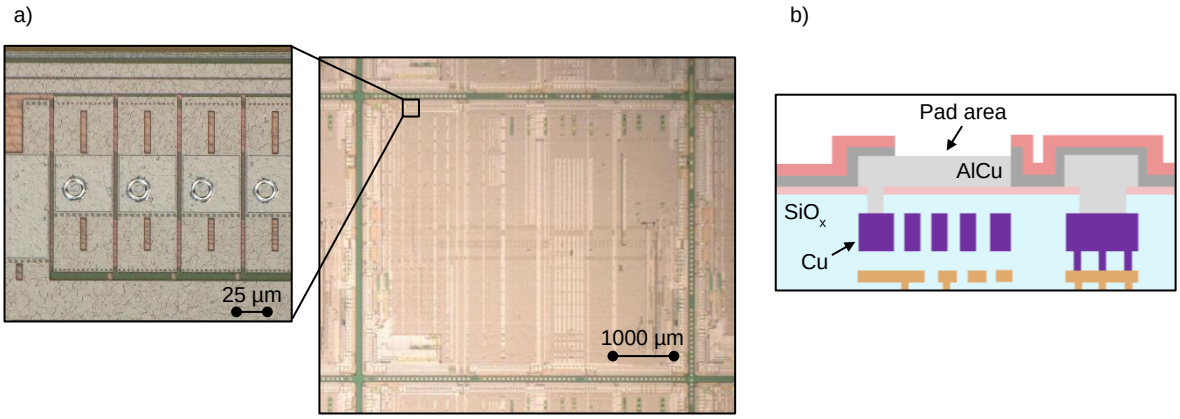

Fig. 9. a) Used test specimen with AlCu (aluminium-copper) probe pads (45 µm x 45 µm) showing imprints of the SI system in Fig. 1 (10 µm tip diameter, 300 mN maximum contact force). b) Schematic stack layout under the contact pad. The structures are not drawn in scale.

The tip size and the maximum applied load are kept identical in the repeated crack analysis using also a 10 µm diameter tip and around 300 mN maximum contact force. In Fig. 10 the comparative measurement data obtained after 120 contact cycles with the dual cantilever is displayed. The cantilever design leads to a different imprint shape with an added scrubbing motion (Fig. 10d)). The general distribution of the AE hits (Fig. 10a)) is similar to the previous test run with a slight shift of the 1st filtered crack signals to higher force values.

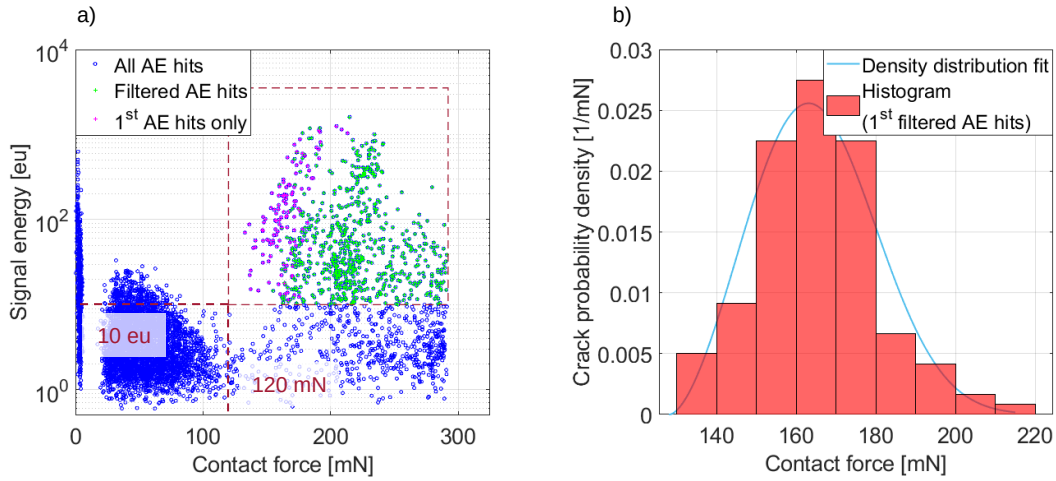

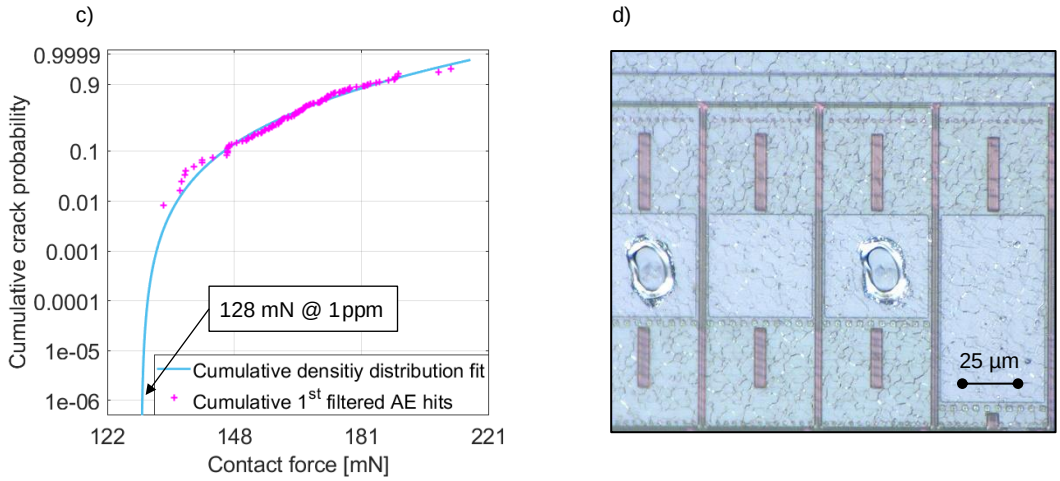

Fig. 10. Measurement results after 120 contact cycles on the probe pads in Fig. 9 with the dual cantilever in Fig. 3 (bending stiffness: 1.5 mN/µm). a) Filtered AE crack signals (limits: 10 eu and 120 mN). b) Measured crack probability density including a distribution fit. c) Measured cumulative crack probability including a distribution fit. Extrapolated crack probability of 1 ppm at 128 mN contact force. d) Image of the generated probe marks on the contact pads (about 11 µm scrub length).

Following the same steps as in Fig. 8, the calculation of the contact force limit with a 1 ppm crack probability leads to a value of 128 mN. To check the influence of the added scrubbing motion, the measurement series is repeated with a different cantilever design with increased bending stiffness (3.6 mN/µm vs. 1.5 mN/µm) and reduced scrub length (4 µm vs. 11 µm). The corresponding signal evaluation leads to a reduced contact force limit at 105 mN, displayed in Fig. 11. No clear correlation between the scrub length and the contact force limit can be derived, as the old measurement setup with no scrubbing at all had a medium load limit of 117 mN. The shapes of the density distributions obtained with the new cantilever design in Fig. 10b) and Fig. 11b) are quite different. In the last one, the left arm is more accented which leads to an extended crack probability into lower contact force values in Fig. 11c). With only 120 load cycles and extracted data points, the distribution fits and the extrapolations of the crack probabilities to a value of 1 ppm are too sensitive to possible outliers. To exclude this risk, the test runs with the new setup need to be repeated with a higher contact cycle number. In general, the manual selection of the filter boundaries, especially the force limit, causes the risk of creating an artificial, lower boundary for the crack probability. This can cause a steeper drop of the crack probability distributions and increased contact force limits. An automatic filter algorithm including other signal features would be favourable.

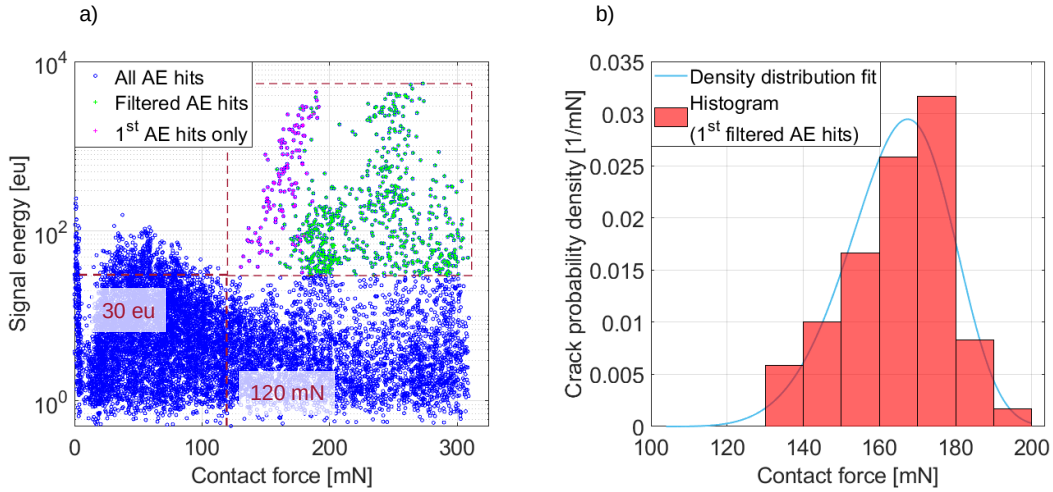

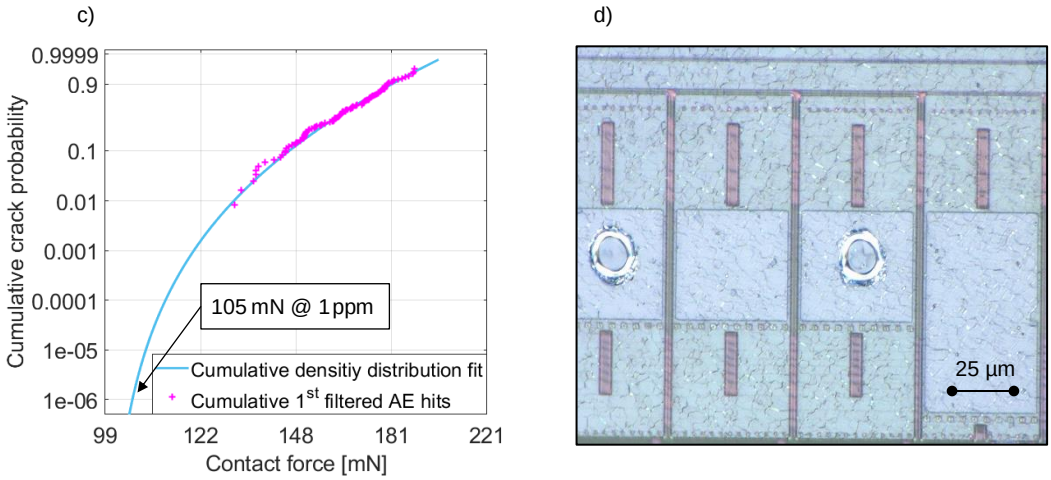

Fig. 11. Measurement results after 120 contact cycles on the pads in Fig. 9 with a more rigid dual cantilever geometry (bending stiffness: 3.6 mN/µm). a) Filtered AE crack signals (limits: 30 eu and 120 mN). b) Measured crack probability density including a distribution fit. c) Measured cumulative crack probability including a distribution fit. Extrapolated crack probability of 1 ppm at 105 mN contact force. d) Image of the generated probe marks on the contact pads (about 4 µm scrub length).

What also catches the eye is that there is a gap of recorded AE signals at low force values in Fig. 10a) and Fig. 11a). The width of this gap seems to correlate with the low bending stiffness of the cantilever designs. The measurement series with the stiffer cantilever in Fig. 11a) has a smaller gap. In general, the cantilever designs which provide a softer mounting of the indenter compared to the SI system (7.4 mN/µm), combined with the small wafer prober vibrations (Fig. 7), seem to cause a slight oscillation of the indenter tip. This tip movement prevents a transmission of the AE signals at the beginning of the contact cycles. This effect doesn't influence the crack probability calculation as it only happens at very low contact force values. Analysing the signal energy spans of the recorded AE hits, there can be seen a drop of about 20 to 30 dB between the old measurement setup (Fig. 8a)) and the new measurement setup (Fig. 10a) and Fig. 11a)). As the AE trigger threshold is adjusted to the noise floor, this also correlates to the signal-to-noise ratios (SNRs) of the test runs. Earlier comparisons [7] only showed a decrease of around 10 dB between the two setup variants. The additional loss of 10 to 20 dB SNR in more recent tests could be caused by a degradation of the AE signal transmission line. The connection from the AE piezo element to the PCB (Fig. 3) uses a conductive adhesive (*M&G Chemicals, 8331D* [11]) that maybe worsens over time. Also, the applied micro coaxial cable (*Hirose Electric Co., U.FL-2LPHF6* [12]) is only specified for 30 mating cycles, which may already have been reached by the time of performing the crack probability analyses.

4. Conclusion and Outlook

The mechanical load limit of semiconductor devices plays an important role to perform their functionality check during wafer testing without damaging them. A measurement setup is used that defines these load limits by overloading the test substrates intentionally with an indenter and detecting the generated cracks with help of the emitted AE signals. In this study a new sensor solution has been developed that allows to perform the crack probability tests inside a wafer prober. This enables measurement conditions as close as possible to the productive test environment with more accurate end results. To check the applicability of the wafer prober integration, crack probability analyses are repeated on the same test specimen with the old and new measurement setup. The evaluation of the AE data leads to similar contact force limits with a crack probability of 1 ppm between 105 and 128 mN. This proves

the general functionality of the developed test bench and the applicability of an AE-based crack detection method inside a wafer prober.
The results also show some room for further improvements and investigations. No clear correlation between the scrub length of the imprint and the contact force limit could be detected yet. For future test runs, a higher number of contact cycles will be used to generate a sufficient data base for an extrapolation to a 1 ppm crack probability. To make the fit of the distribution functions more stable, an automatic filtering algorithm of the AE crack signals would be preferable compared to the current manual selection of filter limits. With the new measurement setup, after the first contact between indenter and substrate, no AE hits are recorded for a short period of time. This seems to be caused by the softer indenter suspension combined with small, mechanical vibrations inside the wafer prober. Comparing the SNRs of the AE signals, a decrease of 20 to 30 dB can be seen with the new setup. Previous tests only have shown a 10 dB reduction. The additional SNR loss could be caused by a recent deterioration of the AE signal transmission (micro coaxial cable or conductive adhesive).

References

[1] N. Faisal, R. Ahmed and R. Reuben, "Indentation testing and its acoustic emission response: Applications and emerging trends," *International Materials Reviews,* vol. 56, no. 2, pp. 98-142, 1 March 2011, 10.1179/1743280410Y.0000000004.

[2] P. Dyjak and R. Singh, "Acoustic emission analysis of nanoindentation-induced fracture events," *Experimental Mechanics,* vol. 46, pp. 333-345, 27 March 2006, 10.1007/s11340-006-7303-x.

[3] N. Tymiak, A. Daugela, T. Wyrobek and O. Warren, "Acoustic emission monitoring of the earliest stages of contact-induced plasticity in sapphire," *Acta Materialia,* vol. 52, no. 3, pp. 553-563, 9 February 2004, 10.1016/j.actamat.2003.09.039.

[4] M. Unterreitmeier, "Contact related failure detection of semiconductor layer stacks using an acoustic emission test method," Ph.D. dissertation, Dept. of Eng., FAU Univ., Erlangen, Germany, 2020.

[5] O. Nagler, S. Bernrieder and M. Unterreitmeier, "System and method for examining semiconductor substrates". United States Patent US 10,859,534 B2, 8 December 2018.

[6] M. Unterreitmeier, O. Nagler, L. Pfitzner, R. Weigel and R. Holmer, "An acoustic emission sensor system for thin layer crack detection," *Microelectronics Reliability,* vols. 88-90, pp. 16-21, September 2018, 10.1016/j.microrel.2018.07.015.

[7] F. Tremmel, O. Nagler, C. Kutter and R. Holmer, "Dual cantilever probe for crack probability analysis of multilayer substrates during wafer probing," *IEEE Sensors Journal,* 2025 (under review).

[8] *Vallen AE Suite Software Manual,* Vallen-Systeme GmbH, Wolfratshausen, Germany, 2011, p. 41.

[9] A. C. Fischer-Cripps, „Statistics of brittle fracture," in *Introduction to Contact Mechanics*, New York, Springer Science+Business Media, 2007, pp. 64-67, 10.1007/978-0-387-68188-7_4.

[10] M. Unterreitmeier and O. Nagler, "An improved crack probability model for silicon oxide layers using three-parameter Weibull analysis," *Microelectronics Reliability,* vol. 150, November 2023, 10.1016/j.microrel.2023.115193.

[11] *8331D - Silver Conductive Epoxy Adhesive,* M&G Chemicals, Burlington, Canada, [Online]. Available: https://mgchemicals.com/products/adhesives/electrically-conductive-adhesives/silver-epoxy/. [Accessed 29 July 2024].

[12] *U.FL Series,* Hirose Electric Co., Tokyo, Japan, [Online]. Available: https://www.hirose.com/en/product/series/U.FL. [Accessed 29 July 2024].